Pflügers Arch - Eur J Physiol (2001) 443:132–145
DOI 10.1007/s004240100631

ORIGINAL ARTICLE

M. I. Glavinović · H. R. Rabie

Monte Carlo evaluation of quantal analysis in the light of Ca^{2+} dynamics and the geometry of secretion

Received: 19 February 2001 / Revised: 11 May 2001 / Accepted: 28 May 2001 / Published online: 12 July 2001

Abstract Using the Monte Carlo technique, Ca^{2+} dynamics were simulated in the absence and presence of vesicles to gain better insight into what governs quantal release. A vesicle, represented as a flat, infinitely thin surface, was positioned parallel to the plasma membrane at a chosen distance from the locus of Ca^{2+} entry. Because vesicles act as important diffusion barriers after the synchronous opening of Ca^{2+} channels (as occurs during evoked release), $[Ca^{2+}]$ close to the plasma membrane reaches higher levels than it would in the absence of vesicles. The rise in $[Ca^{2+}]$ is greater under larger vesicles close to the plasma membrane, which thus have a higher probability of release. The power–law relationship between the $[Ca^{2+}]$ and the probability of release, and the cubic relationship between the vesicular diameter and its volume can make this relationship very steep. In contrast, when release occurs owing to fluctuations of $[Ca^{2+}]$ – as a result of Ca^{2+} release from an internal store or asynchronous opening of Ca^{2+} channels (during spontaneous release) – the effect of vesicles as diffusion barriers is less pronounced and vesicles of different sizes should have a similar probability of release. Since the preferential release of large vesicles depends on how the Ca^{2+} needed for secretion is raised (synchronously versus asynchronously), the quantal size of evoked and spontaneous release should differ. The main factors influencing the preferential release of large vesicles are the distance between vesicles and the plasma membrane, the concentration of Ca^{2+} buffers, and single-channel Ca^{2+} flux. Vesicles also have a pronounced effect on Ca^{2+} binding to buffers and on the spatio-temporal distribution of bound buffers. The greater the vesicular size and the closer their position to the plasma membrane, the more fixed buffers will be bound near the plasma membrane because of limited diffusion of Ca^{2+}. Since bound fixed buffers act as "memory elements", such a change in their spatial distribution will further enhance the probability of release of large vesicles during stimulation.

Keywords Monte Carlo simulation · Calcium dynamics · Quantal analysis · Quantal size · Vesicular secretion

M.I. Glavinović (✉)
Department of Anaesthesia Research, McGill University,
3655 Drummond Street, Montreal, P.Q. H3G 1Y6, Canada
e-mail: mladen@med.mcgill.ca
Tel.: +1-514-3986002, Fax: +1-514-3987452

H.R. Rabie
Department of Applied Chemical and Biological Sciences,
Ryerson Polytechnic University, Toronto, ON, Canada

M.I. Glavinović
Department of Physiology, McGill University, Montreal PQ, Canada

Introduction

The first evidence that secretion occurs in multi-molecular quantal packets was presented half a century ago [20, 25], which led to the now widely used methodology of quantal analysis [20]. In its original form the analysis requires measurement of the amplitudes of both the evoked responses and spontaneously released quanta and rests on the assumption that the amplitudes of evoked unitary events and spontaneously released quanta have the same mean value and the same variance. However, even when identical, the quantal size of evoked and spontaneous quanta are expected to differ. Unlike the spontaneous events, the apparent quantal size (the inter-peak distance in amplitude histograms) of evoked events is reduced because of the time dispersion of synaptic delays [64, 73]. Direct experimental evidence about quantal size from the adult neuromuscular junction is available only under restricted conditions (low Ca^{2+}/Mg^{2+} levels of the bathing medium). At physiological levels of release [14, 30, 31] at adult synapses and at developing synapses [21, 22], the evidence suggests that such a correspondence does not always hold. At central synapses the mean size (though not necessarily the mode) and distribution of spontaneous events often differ from the quantal size and the variance underlying evoked events [7, 8, 9, 24, 41, 74]. Taken together the evoked quanta may have not only a smaller [31, 41] but also greater quantal size [14, 21, 22, 31]. The quantal

composition of evoked synaptic currents can sometimes [24, 41, 53], but not always [8, 9], be inferred from multiple equidistant modes. If multimodal peaks in the amplitude histograms of evoked events are clearly present, the quantal analysis can proceed without making assumptions about spontaneous events [45, 46]. Finally, the multimodal equidistant peaks can also sometimes [24, 53, 54, 74], though not always [8, 9, 41] be observed in amplitude histograms for spontaneous events. There is surprisingly little understanding of what may regulate the difference in quantal size of evoked and spontaneous release.

Most secretory cells use Ca^{2+} entry as a link between stimulation and secretion. In this study, using Monte Carlo simulation methods, we examine theoretically whether the differences in the quantal size of evoked and spontaneous release are due to underlying differences in Ca^{2+} dynamics. Several studies have modeled Ca^{2+} dynamics in very small compartments around the Ca^{2+} channels to evaluate the role of Ca^{2+} dynamics in determining the time course of transmitter release at the nerve terminal [13, 42, 43, 56, 60, 76, 77]. They led to the notion of Ca^{2+} micro-domains of >100 μM developing rapidly after the opening of the Ca^{2+} channel and collapsing within several microseconds after a channel closure [47, 60]. In addition, models have been developed to assess the role of Ca^{2+} buffers [49, 51, 56, 62, 75]. It is now clear that the evaluation of the free-Ca^{2+} gradients under the membrane is critical for understanding the relationship between Ca^{2+} entry and secretion [18, 43]. There has been no systematic evaluation of how Ca^{2+} dynamics are affected by the presence of secretory vesicles. In this study, we focus our attention on the changes in sub-membrane Ca^{2+} dynamics caused by the presence of vesicles: the goal is to identify the rules governing quantal release in such secretory cells under a variety of conditions.

There are several reasons for adopting Monte Carlo simulation instead of diffusion-reaction differential equations when assessing Ca^{2+} dynamics. First, the Monte Carlo simulation gives both average values of the variables of interest and also information about their variability. Second, no assumptions are made about the symmetry or linearity of the process. Third, this method is highly suitable for studying diffusion in systems with complex geometry and more easily takes into account the boundary conditions.

A preliminary account has appeared as an abstract [33].

Simulation methods

Theory

Calcium dynamics were simulated by the Monte Carlo method [6, 32, 72]. At each discrete time step, every Ca^{2+} ion is associated with a position, and is either flagged as free or bound. Free Ca^{2+} ions move randomly in all three dimensions or interact with buffers. Buffer molecules are positioned equidistantly on a rectangular grid and their position is fixed. Every buffer molecule has a finite probability of changing to another state according to the same kinetic scheme that has one forward binding and one backward unbinding rate. The changes of the buffer states depend only on their present position and not on their previous history (i.e., they are Markovian).

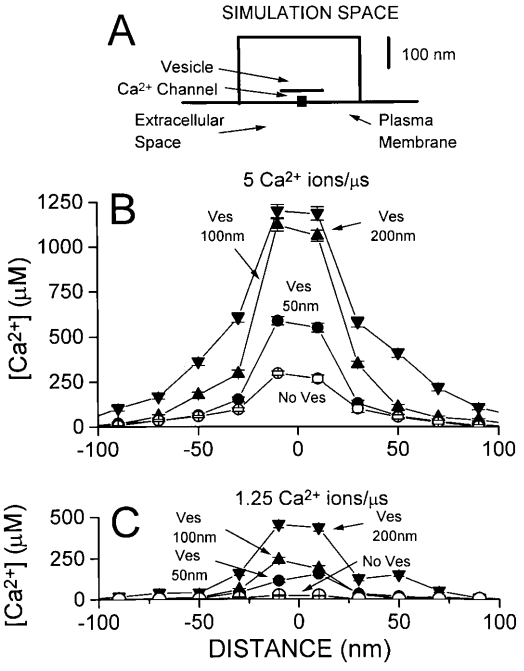

Fig. 1 **A** Simulation space approximately to scale. Dimensions were 400×400×200 nm. Ca^{2+} entered in the middle as indicated. Flat infinitely thin diffusion barriers, with variable dimensions and position, were taken as "vesicles". Ca^{2+} entered from a hemisphere with a 89.4 nm radius through a pore 5 nm long. Ca^{2+} flux was regulated by changing the pore diameter (see Simulation methods). **B**, **C** The presence of vesicles markedly changes the free [Ca^{2+}] spatial profiles in a 15 nm thin layer near the plasma membrane estimated 300 μs from the start of simulation and Ca^{2+} entry. In two cases shown either there was no diffusion barrier present (*No Ves*), or they were present (their dimensions were as indicated) and were positioned 15 nm above the plasma membrane. Ca^{2+} entered at the origin (x=0) and its flux was 5 ions/μs (**B**) or 1.25 ions/μs (**C**)

Computer simulations

All simulations were done using MATLAB. Since the resolution of the processes examined is of the order of 1–10 μs, the time step in our simulation was 0.2 μs [43, 58]. Individual points shown in figures are mean values and the horizontal parallel lines are standard errors. The following are different components of the simulation of buffered Ca^{2+} dynamics in the presence of vesicles.

Geometry of simulations

A rectangular box (400×400×200 nm) was chosen as a simulation space (Fig. 1A). Diffusion in the simulation space was calculated by assuming that Ca^{2+} ions collided elastically with the "walls" of the space (the vesicle or the plasma membrane). Collisions are considered as elastic when the velocity of the rebound is equal to the initial velocity (i.e. the velocity prior to the collision). The vesicle was represented as a flat, infinitely thin rectangular surface positioned at a chosen distance from the plasma membrane and parallel to it. Although a flat rectangular surface is less representative of the physiological situation, it was chosen instead of a sphere to

Table 1 Parameters for simulations

	Value	Comment
Calcium		
Basal $[Ca^{2+}]_I$	100 nM	
Diffusion constant (intracellular)	220 $\mu m^2 s^{-1}$	[2]
Diffusion constant (extracellular)	800 $\mu m^2 s^{-1}$	
Calcium entry		
Calcium flux	5 ions/μs	This is approximately equivalent to 1.6 pA
Ca^{2+} channel pore length	5 nm	
Ca^{2+} channel pore diameter	1 nm	
Fixed buffer		
Forward binding rate	5×10^8 $M^{-1}s^{-1}$	[29, 35]
Concentration	360 μM	Concentration and affinity are chosen, so that κ=41
Dissociation constant	10 μM	[43]
Unbinding rate	5,000 s^{-1}	Calculated from the dissociation constant and forward rate

All parameters except those describing calcium basal concentration and its diffusion constant and the calcium channel pore length were varied in our simulations

simplify and speed up the numerical evaluation. The pore was represented as a cylinder 5 nm long and with a radius of 1 or 2 nm (see below). The plasma membrane was infinite in size and was "impermeable" to internal or external Ca^{2+} ions. In contrast Ca^{2+} ions could move across other "walls" of the simulation space, but fixed buffers were present only within the simulation space. This choice was made because restricting the movement of Ca^{2+} ions to the simulation space made very little difference to the process studied. This is not surprising given that very few Ca^{2+} ions reach the end of the simulation space within the simulation time that typically lasted 200–300 μs (Table 1).

Diffusion

The diffusion of Ca^{2+} ions is modeled as a random walk. At each time step, the distance traveled by a Ca^{2+} ion (in each of three dimensions) was chosen randomly from a Gaussian distribution with mean of 0 and a standard deviation σ given by:

$$\sigma=\sqrt{2D\delta t} \quad (1)$$

where δt is the length of the time step and D is the diffusion coefficient of Ca^{2+} ions. The diffusion coefficient of Ca^{2+} ions in water is 600 $\mu m^2/s$ [57], but in buffer-free cytoplasm of oocytes it was taken as 220 $\mu m^2/s$ [2].

Kinetics of Ca^{2+} buffering

A volume and a probability of binding are associated with the free or unbound state of the buffer molecule, assuming that Ca^{2+} "hits" this volume [6, 32, 72]. The inverse of the fixed buffer volume is the density of the buffer molecules (σ_r) per unit volume. The probability (P_b) that a Ca^{2+} ion, after hitting this volume, will bind in a given time step (δt) is related to the macroscopic rate constant by:

$$P_b=[(\sigma_r\kappa)/N_a]\sqrt{(\pi\delta t)/D} \quad (2)$$

where N_a is Avogadro's number and κ the forward rate (in M^{-1} s^{-1}). For the unbinding step in the kinetic scheme, the probability (p) of unbinding is related to the macroscopic (backward) rate constant by:

$$p=1-e^{-k\delta t} \quad (3)$$

where k is the backward rate constant (in s^{-1}). The forward and the backward rate constants were 5×10^8 M^{-1} s^{-1} and 500 s^{-1} respectively or as otherwise specified [29, 35, 43]. This yields a dissociation constant of 10 μM [43]. The affinity of fixed as well as mobile buffers is low in chromaffin cells (K_D appears to be >5 μM; [41]). We chose K_D value of 10 μM in our simulations but higher affinity buffers were also used whose K_D values were 1 or 0.1 μM. In such cases either the off rate was lowered or the on rate raised accordingly. The concentration of fixed buffer was 360 μM (or as otherwise specified). This yields a "convenient" number of fixed buffer molecules (24×24 for a total of 576 in a "single layer" of 400×400 nm or 6912 in the whole three-dimensional simulation space) but is 16% higher than used by Klingauf and Neher [43]. This is equivalent to a separation of 16.7 nm between individual buffer molecules. In the whole simulation space there are thus 12 layers 16.7 nm apart.

Initial and boundary conditions

All simulations started with $[Ca^{2+}]_i$ at 0.1 μM. For simplicity all fixed buffers were assumed to be free initially, although approximately 1% of all fixed buffers would be expected to be in the bound state given the initial free $[Ca^{2+}]$ and the total binding ratio κ (the ratio of bound to free $[Ca^{2+}]$) of endogenous buffers of 41 in chromaffin cells [78]. In other secretory cells with a higher binding ratio, this assumption of very low fraction of fixed buffers being in the bound state under resting conditions would be less valid. In isolated rat neurohypophyseal nerve endings, the total binding ratio κ has been estimated to be 174 [67], while it is 600 at the crayfish neuromuscular junction [69]. The binding ratio will also change with experimental conditions (e.g., increasing with large Ca^{2+} load; [67]). Furthermore the binding ratio changes with cell development, because the expression of Ca^{2+} buffers is developmentally regulated [28, 48]. Ca^{2+} ions could enter only through the "pore". Though "calcium-induced calcium release" from internal stores after individual depolarizations inducing secretion may be important, they are not expected to be an important factor on the time scale of our simulations [50].

The single-channel Ca^{2+} flux was assumed to be 5 or 1.25 ions/μs. This is approximately equivalent to 1.6 pA and 0.4 pA respectively. Ca^{2+} ions entered into the cell from a small "extracellular" hemi-sphere whose radius was 89.4 nm, and which had a constant number of Ca^{2+} ions irrespective of Ca^{2+} efflux. This radius corresponds to five mean diffusion lengths for a Ca^{2+} ion in the extracellular space (assuming an extracellular diffusion constant of Ca^{2+} of 800 $\mu m^2/s$). This approach does not take into account: (1) that the entry of Ca^{2+} ions is governed not only by the concentration but also by the electrical gradient, and (2) any binding-unbinding ion interactions in the pore. It was nevertheless used to simplify the simulation of desired Ca^{2+} fluxes. The single-channel Ca^{2+} fluxes of 5 or 1.25 ions/μs were obtained with the 1- and 2-nm pore radii. Note that a twofold change of pore radius leads to a fourfold change of Ca^{2+} fluxes (the flux being proportional to the cross-sectional area of the pore).

For several reasons we varied the single-channel Ca^{2+} fluxes. Experimental evidence has revealed a variety of Ca^{2+} channels (L, N, T, P/Q types) with differing single-channel conductances.

For bovine chromaffin cells noise analysis gives estimates of single-channel current of 0.03 pA at +10 mV for 1 mM $[Ca^{2+}]_o$, which is expected to yield ≅0.06 pA for 2 mM $[Ca^{2+}]_o$. For chick ciliary ganglion neurons and 2 mM $[Ca^{2+}]_o$ the single-channel current is 0.15–0.2 pA at –10 mV [15]. Furthermore for a chromaffin cell with a diameter of 15 µm, the depolarization-induced whole-cell Ca^{2+} current is typically 500 pA, yielding an "average" current density of 0.71 pA/µm². At the active zones of synapses, these values are expected to be much higher. In previous simulations of hair cells, 85 Ca^{2+} channels were assumed on a presynaptic surface of 0.25 µm² [56]. With 12% probability of opening, this yielded 8 pA or 32 pA/µm² (tenfold lower Ca^{2+} fluxes were also simulated). Our values fall in between: they were 10 and 2.5 pA/µm².

We assumed that Ca^{2+} enters through a single channel. This is reasonable given the dimensions of the simulation space and the nature of the questions being asked. Furthermore, the channel density has been estimated at 5–15 channels per µm² in chromaffin cells [26], which amounts to 300 nm separation between channels, yielding approximately 1–2 channels in our simulation space (a higher density would be expected on the basis of the estimate by Artalejo et al. [4]).

Other conditions

Extrusion processes and internal stores were not included in simulations. They are not expected to be important as sinks (or sources) of Ca^{2+} on the time scale of our simulations for the following reasons. Assuming the forward binding rate of the plasma membrane Ca^{2+} pump to be 10^7 M^{-1} s^{-1}, V_{max}=5 pM cm^{-2} s^{-1} and Michaelis–Menten constant K_M=0.83 µM [58, 78], one obtains an unbinding rate of 3.3 s^{-1}, a second forward rate of 10 s^{-1} and a concentration of 3 $µm^{-2}$. This amounts to a low rate of extrusion per transport molecule and less than one molecule extruded from the simulation space. A similar argument applies to the internal extrusion processes, assuming the same concentration, forward and backward binding rate as for external extrusion.

Results

Effect of vesicular presence on spatial distribution of Ca^{2+} near the plasma membrane

Figure 1 gives two families of spatial concentration profiles of free $[Ca^{2+}]$ in a 15-nm-thick layer near the plasma membrane in the presence and absence of vesicles. Vesicles, represented as flat rectangular surfaces, were barriers to diffusion of Ca^{2+} and were positioned 15 nm above the plasma membrane. Morphometric studies have shown that the distances between the plasma membrane and the docked vesicles prior to secretion are often in this range [52, 65], but greater distances were also used (see below). The dimensions of the flat surfaces were as given (100 nm indicates 100×100 nm rectangular flat surface). They varied in size over a wide range (from 25 to 400 nm). This spans the whole range of vesicular diameters both in synapses (peripheral and central) and in neuroendocrine cells [12, 19, 34]. Such a wide range was also chosen to facilitate the examination of the relationships and trends that exist among the variables of interest that may be present but not necessarily prominent, and that could be overlooked owing to the stochastic nature of Monte Carlo simulations.

Free $[Ca^{2+}]$ was calculated as a mean value over an interval 10 µs long 290–300 µs from the start of simulation. Ca^{2+} entered throughout the simulation (i.e., for 300 µs; this was also a typical total duration for our simulations). This duration of Ca^{2+} entry was chosen since the mean open time of a single Ca^{2+} channel is expected to be of that order. In chromaffin cells the mean open time has been estimated from noise analysis at ≅1 ms [26]. In the presence of Bay K 8644 the Ca^{2+} channel, which is active at potentials of –30 mV and above (L-type), has two dominant modes with characteristic time constants 0.5 and 5 ms [10, 11]. We evaluated the free $[Ca^{2+}]$ at the same chosen time rather than evaluating their steady-state values. This approach is felt as justified given that the questions being addressed are related to the understanding of relationship between the Ca^{2+} dynamics and quantal analysis. During the time interval from the start of the Ca^{2+} entry to the moment when Ca^{2+} ion binds to the release trigger molecule, the Ca^{2+} steady-state level will be reached to a different extent in different cases depending on a variety of factors – the presence of diffusion barriers (their size and positioning), single-channel Ca^{2+} current flux and the concentration, kinetics and affinity of Ca^{2+} buffers (see below). We evaluated the effect of the vesicular presence on the Ca^{2+} spatial profiles for two different single-channel Ca^{2+} fluxes – 5 ions/µs (Fig. 1B) or 1.25 ions/µs (Fig. 1C) corresponding to single-channel currents of 1.6 and 0.4 pA respectively. We varied the single-channel current to determine how the spatial concentration profiles of free Ca^{2+} are altered with a change in the extracellular Ca^{2+} concentration or with Ca^{2+} entering through channels with differing single-channel conductance.

Free Ca^{2+} profiles are clearly spatially very constrained. Their decline with distance has a space constant of approximately 50 nm. However, this is mostly because the steady-state levels are only partially reached. With a steady-state reached, the free Ca^{2+} profiles are less spatially restricted since the time needed to reach the steady-state is greater for more distant areas (see Fig. 9). The presence of diffusion barriers clearly increases free $[Ca^{2+}]$ in the thin layer near the plasma membrane, and more so the greater the size of the diffusion barrier. Though the increase in $[Ca^{2+}]$ induced by the vesicular presence is relatively greater at larger distances, it is evident very near the locus of Ca^{2+} entry and for both Ca^{2+} fluxes chosen. Since Ca^{2+} is a link between the depolarization and release, greater accumulation of free Ca^{2+} under large vesicles suggests that larger vesicles will be preferentially released even in synapses with good co-localization between the Ca^{2+} channels and vesicles. Furthermore a comparison of these two families of concentration profiles suggests that the importance of vesicles in altering the spatio-temporal distribution of free $[Ca^{2+}]$ depends on the single-channel Ca^{2+} flux. Preferential release of large vesicles may thus depend on the extracellular Ca^{2+} concentration and/or on the type of Ca^{2+} channel involved in secretion.

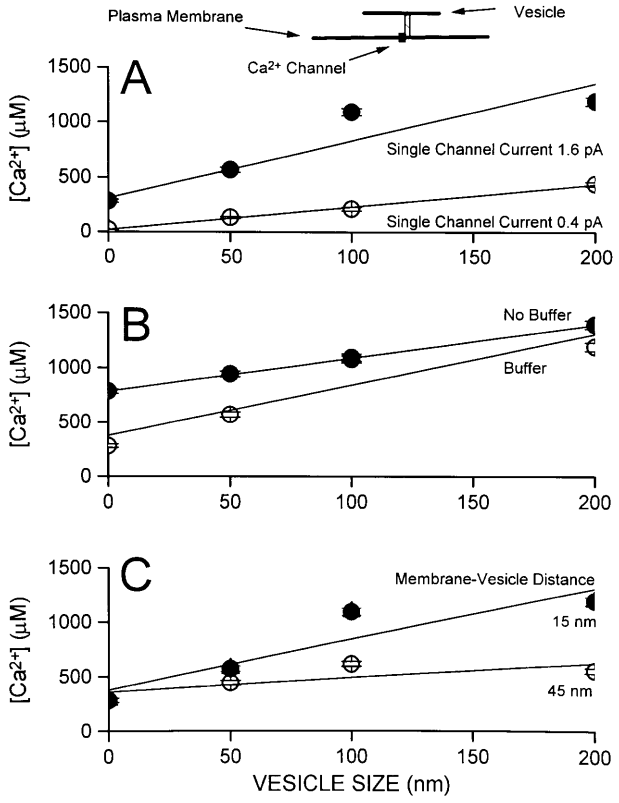

Fig. 2A–C Vesicular presence near the plasma membrane enhances the free $[Ca^{2+}]$ and more so the larger the vesicles. Furthermore, this vesicle-size-dependent increase of the free $[Ca^{2+}]$ depends on: **A** the single-channel current flux, **B** the concentration of fixed buffers, and **C** the separation between the plasma membrane and the diffusion barrier. Free $[Ca^{2+}]$ was estimated 10 nm from the locus of Ca^{2+} entry (see *inset* in **A**), 300 μs from the start of simulation and Ca^{2+} entry. Both overall free $[Ca^{2+}]$ and the vesicle-size-dependent component of the free $[Ca^{2+}]$ rise with greater single-channel Ca^{2+} flux and closer vesicular positioning to the plasma membrane. In contrast free $[Ca^{2+}]$ decreases, but its dependence on the vesicular size increases in the presence of fixed buffers. Ca^{2+} entered at the center (i.e., at x=0) throughout the simulation and its flux was 5 ions/μs (equivalent to 1.6 pA) except in **A** where it was also 1.25 ions/μs (or 0.4 pA). The diffusion barriers were positioned 15 nm from the plasma membrane (except in **C** where it was also 45 nm). The total fixed buffer concentration was 360 μM (or no buffer in **B**)

Factors controlling dependence of free $[Ca^{2+}]$ on the size of vesicles positioned for secretion

We now examine quantitatively the relationship between the free $[Ca^{2+}]$ and the vesicular size under a variety of conditions to determine what regulates the greater accumulation of free Ca^{2+} under large vesicles and thus their preferential release. We focus our attention on the changes in the free $[Ca^{2+}]$ near the plasma membrane very close to the Ca^{2+} entry (10 nm from the locus of Ca^{2+} entry). Figure 2A gives the dependence of free $[Ca^{2+}]$ on the vesicular size for two different single-channel current fluxes of Ca^{2+} (5 and 1.25 ions/μs; same simulation runs as in Fig. 1). As expected, the vesicle-size-independent free $[Ca^{2+}]$ near the plasma membrane is greater for higher single-channel Ca^{2+} fluxes. However, in addition to this "expected" difference, another difference becomes also apparent. The relationship between the free $[Ca^{2+}]$ and the vesicular size is steeper when Ca^{2+} fluxes are greater. The best-fitted lines (calculated using the leastsquares method) were (±SD): y=(19.3±10.7)+[2.1(±0.1)·x] for a single-channel current of 0.4 pA and y=(377±162)+[4.7(±1.4)·x] for a single-channel current of 1.6 pA, where y is the free $[Ca^{2+}]$ (in μM) and x is the vesicular size (in nm). The corresponding P values were 0.002 and 0.08, whilst the correlation coefficients R were 1.0 and 0.92.

Single-channel Ca^{2+} flux however is not the only factor expected to affect the relationship between the $[Ca^{2+}]$ and vesicle size. Both vesicular position and the Ca^{2+} buffer concentration are additional important factors (Figs. 2B, C). The best-fitted lines were (±SD): y=(377±162)+[4.7(±1.4)·x] (fixed buffer present, and single-channel current – 1.6 pA; P and R values were 0.08 and 0.92), y=(786±8)+[3.0(±0.1)·x] (no fixed buffer and single-channel current – 1.6 pA; P and R values were <0.001 and 1.0), y=(357±88)+[1.3(±0.8)·x] (fixed buffer present, single-channel current – 1.6 pA and vesicle-plasma membrane distance 45 nm; P and R values were 0.23 and 0.77) and y=(377±162)+[4.7(±1.4)·x] (fixed buffer present, single-channel current – 1.6 pA and vesicle-plasma membrane distance 15 nm; P and R values were 0.08 and 0.92). Note however that although both the presence of fixed buffers (and generally the concentration of fixed buffers) and the closer positioning of the diffusion barrier to the plasma membrane make the relationship between the free $[Ca^{2+}]$ and the vesicular size steeper, their effects on the vesicle-size-independent free $[Ca^{2+}]$ are opposite. Closer vesicular positioning enhances it while fixed buffers lower it.

Factors controlling the dependence of the size of released vesicles on free $[Ca^{2+}]$

During evoked release and following a synchronized opening of ion Ca^{2+} channels, $[Ca^{2+}]$ will reach higher levels under large vesicles leading to their preferential release. In contrast during spontaneous release the $[Ca^{2+}]$ levels needed for secretion are likely to be reached due to the stochastic fluctuation of $[Ca^{2+}]$ or because of a slow rise in $[Ca^{2+}]$ following a release from internal stores or resulting from entry over a large area of plasma membrane. The vesicles will not be important barriers for Ca^{2+} diffusion and all vesicles will have the same or similar probability of release. We now explore how the size of released vesicles depends on the relationship between $[Ca^{2+}]$ and vesicular size under the assumption that the $[Ca^{2+}]$ needed for secretion remains spatially very restricted (i.e., that it comes exclusively from a channel near the locus triggering secretion irrespective of the single-channel Ca^{2+} flux) to evaluate possible changes of the size of released vesicles over a wide range of secretory conditions.

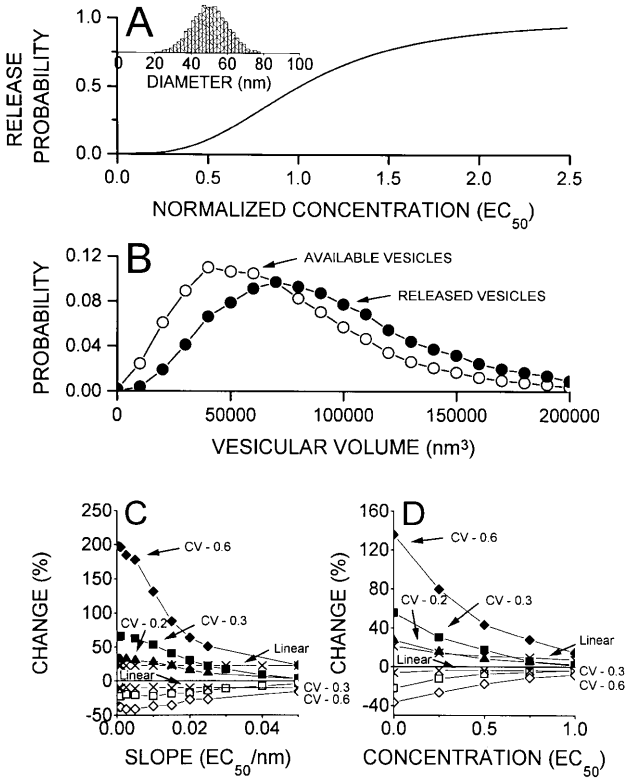

Fig. 3A–D Factors controlling how the size of vesicles released is determined by free [Ca^{2+}]. **A** The relationship between the release probability and [Ca^{2+}] is taken to be sigmoidal with n=3, and the concentration normalized to EC_{50}. The distribution of vesicular diameters was assumed to be Gaussian with a mean diameter of 50 nm and a standard deviation of 10 nm (shown in the *inset*). **B** The distribution of volumes of released vesicles differs from that of available vesicles (see text). **C**, **D** The volumes of released vesicles have higher mean (*filled symbols*) but lower variability (*empty symbols*) when the variability of available vesicles rises (in all cases shown the mean vesicular diameter of available vesicles was 50 nm but its CV ranged from 0.2 to 0.6 as indicated), the slope of free [Ca^{2+}] versus vesicle diameter dependence decreases and the vesicle-independent free [Ca^{2+}] increases (abscissas were normalized to EC_{50}). Though far less pronounced the changes are evident even when the relationship between release probability and [Ca^{2+}] is linear instead of sigmoidal (*crosses*; CV of volumes of available vesicles was 0.3)

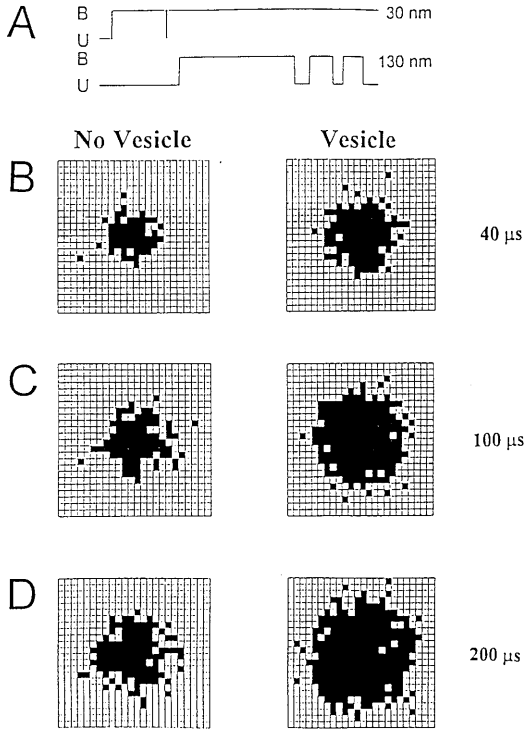

Fig. 4 **A** Time histories of the binding and unbinding of Ca^{2+} to and from two fixed buffer molecules (*B* bound fixed buffer, *U* unbound fixed buffer), both in the "first layer" near the membrane. The distance between the Ca^{2+} channel and the locus of the selected fixed buffer molecule was as indicated on the *right*. The vesicle (200×200 nm) was positioned 15 nm above the plasma membrane. The total concentration of fixed buffer was 360 μM. Ca^{2+} flux was 5 ions/μs (equivalent to 1.6 pA), and occurred throughout the simulation. **B–D** Checkerboard presentation of the stochastic responses of fixed buffers in the "first layer" near the plasma membrane. Each *tile* represents an individual fixed buffer molecule (*black tiles* bound buffers, *white* unbound). Snapshot times were as indicated (40 μs – **A**; 100 μs – **B**; 200 μs – **C**)

Figure 3A shows the relationship (sigmoidal) between the release probability and [Ca^{2+}], with n=3 and the concentration normalized to EC_{50}. The distribution of vesicular diameters (Gaussian with a mean diameter of 50 nm and a standard deviation of 10 nm) is shown in the inset. We calculated the frequency distribution of released vesicles in several steps. First, the frequency distribution of vesicular volumes of available vesicles was determined from the frequency distribution of their diameters (these were, in this and in all other cases, assumed to be Gaussian, but the mean values and the standard deviations of the frequency distributions varied). Second, we calculated the concentration under vesicles of a chosen diameter and assumed that the relationship between the vesicular diameter and the concentration under the vesicle was linear. In each set of calculations the vesicle-size-independent free [Ca^{2+}] and the slope of free [Ca^{2+}] versus vesicular diameter relationship varied. This yields the relationship between the probability of release and the vesicular volume. The frequency distribution of released vesicles was finally determined by multiplying the frequency distribution of available vesicles by the probability of release of vesicles of different volumes and normalizing the so-calculated frequency distribution. As can be seen from Fig. 3B the frequency distribution of volumes of released vesicles differs from that of available vesicles and has a higher mean value. In Fig. 3C, D we show how mean values and the variability of released vesicles is affected by release conditions. Released vesicles always had higher mean values (filled symbols) and lower variability (empty symbols; CV; CV=standard deviation/mean) than available vesicles, but the difference was especially pronounced when the variability of available vesicles rose, and the slope of [Ca^{2+}] versus vesicle diameter relationship (Fig. 3C) or vesicle-independent free [Ca^{2+}] decreased (Fig. 3D). Though far less pronounced, the differences were evident even when the relationship between release probability and [Ca^{2+}] was linear (crosses) instead of sigmoidal.

Stochastic responses of fixed buffers

A full understanding of Ca^{2+} dynamics also requires an understanding of how Ca^{2+} binds to and unbinds from Ca^{2+} buffers and what changes such binding-unbinding produces in the spatio-temporal distributions of the free [Ca^{2+}] and of fixed buffers. Figure 4A gives two time histories of binding and unbinding of Ca^{2+} to and from two individual fixed buffer molecules both positioned near the plasma membrane, but one close (30 nm) and the other further away (130 nm) from the locus of Ca^{2+} entry. Since the simulation step was 0.2 μs all binding-unbinding reactions shorter than 0.2 μs are not shown. The fixed buffer molecule close to the site of Ca^{2+} entry became rapidly bound and remained bound (due to the high free [Ca^{2+}], any unbinding is quickly followed by binding by another Ca^{2+} ion). At a larger distance from the locus of Ca^{2+} entry binding started later and was interrupted by more frequent and longer intervals in the unbound state. Figure 4B–D gives three different "snap-shots" (40, 100, and 200 μs from the start of Ca^{2+} channel opening and of the simulation) of the state of binding of fixed buffers in the "first" layer (i.e., in the layer just near the plasma membrane). The vesicle (a 200×200 nm rectangular flat surface was chosen as a diffusion barrier "representing" the vesicle; see Simulation methods) was positioned 15 nm from the plasma membrane. Not unexpectedly, its presence leads to a faster as well as a greater saturation of fixed buffers in the "first" layer. The saturation also spreads laterally to a much greater extent than in the absence of a vesicle.

Ca^{2+} binding to fixed buffers near the plasma membrane: effect of buffer affinity and vesicular presence

Figure 5A gives the time course of Ca^{2+} binding to fixed buffers in the layer just near the plasma membrane ("first layer"; its dimensions were 400×400×16.7 nm and contained a total of 576 fixed buffer molecules) in the absence of the vesicle and in the presence of vesicles of different sizes as indicated (as previously rectangular flat surfaces were chosen as diffusion barriers "representing" the vesicles) positioned 15 nm above the plasma membrane. In all cases the time course of the number of bound fixed buffers could be well fitted by a single exponential. Though the time needed to reach any level of binding of fixed buffers is shorter in the presence of vesicles, and more so the larger they are, the time needed to reach corresponding half-maximal saturation is not strongly dependent on the vesicular size (Fig. 5B). It is also largely independent of the affinity of fixed buffers for Ca^{2+} irrespective of how the affinity was increased (by increasing the forward rate or by decreasing the backward rate). The best fitted lines (calculated using the least-squares method) were (±SD): t=(48.9±7.6)+[0.11(±0.03)·x], with R=0.84 and P=0.036 (the dissociation constant of the fixed buffer K_D=10 μM); t=(65.7±7.1)+[0.07(±0.03)·x], with R=0.73 and P=0.10 (K_D=0.1 μM, increased by decreasing the unbinding rate hundred times); t=(57.2±15.0)+[0.12(±0.07)·x], with R=0.66 and P=0.15 (K_D=0.1 μM, increased by increasing the binding rate hundred times), where t is the time needed to reach half saturating concentration in μs and x is vesicular size in nm. The insensitivity of the time course of Ca^{2+} binding to fixed buffer to the buffer affinity is not entirely surprising given that the free [Ca^{2+}] is well above K_D. In contrast the "steady-state" values of the bound fixed buffers were strongly dependent on the vesicular size increasing approximately linearly with the vesicular size (Fig. 5C). The best fitted lines were (±SD): N=(77.2±26.5)+[1.2(±0.1)·x], with R=0.98 and P=0.0006 (buffer affinity K_D=10 μM); N=(120.9±33.8)+[1.2(±0.2)·x], with R=0.97 and P=0.001 (K_D=0.1 μM; increased by decreasing

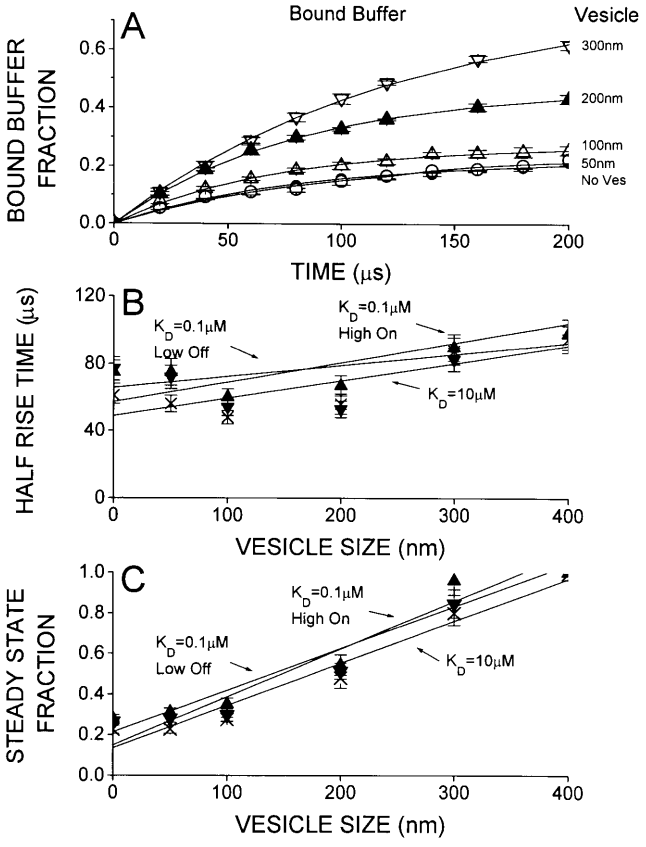

Fig. 5 **A** The presence of diffusion barriers alters Ca^{2+} binding to fixed buffers near the plasma membrane ("first layer"). The *lines* are the best-fitted mono-exponentials. **B** The kinetics of Ca^{2+} binding (given by the half-rise times and evaluated as the times needed to reach the corresponding half steady-state values) are only marginally dependent on the size of diffusion barrier or the marked (a hundred-fold) increase in affinity of the fixed buffer to Ca^{2+}. **C** In contrast the steady-state values of the number of bound fixed buffers strongly depend on the vesicular size, but are largely independent of the buffer affinity to Ca^{2+}. The "total" concentration of fixed buffers (the sum of free and bound fixed buffers) was 360 μM or 576 molecules per layer. Ca^{2+} flux was 5 ions/μs (equivalent to 1.6 pA), and occurred throughout the simulation. K_D of fixed buffers was 10 μM (*crosses*) or 0.1 μM (*filled triangles*). A hundred-fold increase in affinity was achieved either by lowering the off rate (*filled upward triangles*) or raising the on rate (*filled downward triangles*)

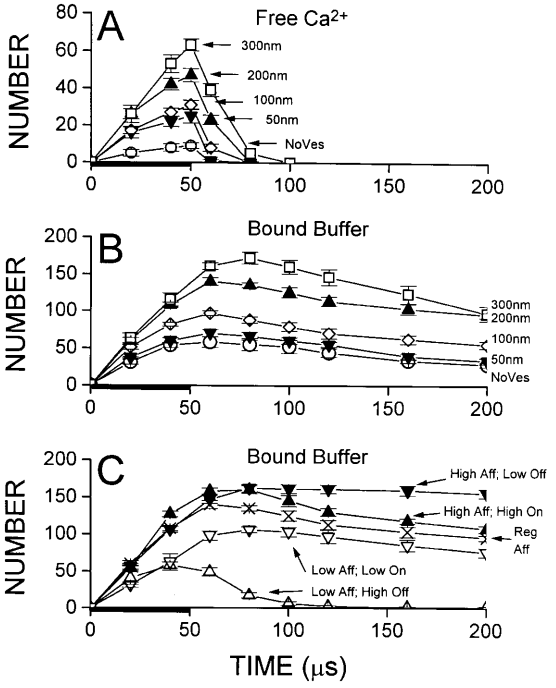

Fig. 6A–C Bound fixed buffers are integrators of Ca^{2+} pulses. The integration depends on the buffer affinity and on the vesicular size. **A** Both the rise and fall of the number of free Ca^{2+} ions near the plasma membrane ("first layer", 15 nm thick) is very rapid. **B** The rise is fast but the fall of the number of bound fixed buffers near the plasma membrane ("first layer", 16.7 nm thick) is slow. Ca^{2+} binding to fixed buffers continued after the closure of the Ca^{2+} channel and depended strongly on the vesicular size. **C** Binding to and especially un-binding from fixed buffers strongly depends on the affinity of fixed buffers. K_D was 1, 10 or 100 μM (corresponding to the high, regular, and low affinity). K_D was changed either by changing the off or on rate (as indicated). Diffusion barriers (200×200 nm) were positioned 15 nm above the plasma membrane. A total of 576 fixed buffer molecules (free and bound) was present per individual layer. Ca^{2+} flux was 5 ions/μs (equivalent to 1.6 pA) and lasted for 50 μs from the start of simulation as indicated by the *horizontal bars*

the unbinding rate hundred times); N=(85.6±36.8)+[1.3(±0.2)·x], with R=0.97 and P=0.001 (K_D=0.1 μM; the binding rate was increased 100 times), where N is the number of bound fixed buffers in the steady-state (the total number of fixed buffers is 576). In all cases the single-channel Ca^{2+} current was 1.6 pA.

Ca^{2+} binding and unbinding to fixed buffers during and following brief fluxes

Figure 6A and B gives the time course of the rise and fall of the free [Ca^{2+}] (note that one Ca^{2+} ion is equivalent to 0.7 μM) and of the number of bound fixed buffers in the "first layer" near the plasma membrane. Note the similarities and differences of their time course. The rise time of both the free [Ca^{2+}] and the number of bound fixed buffers are similarly fast, which shows that the equilibration time of the fixed buffer is much shorter than the diffusion time for Ca^{2+} across a region where most of the Ca^{2+} gradient occurs. The rise of free [Ca^{2+}] is followed by a rapid decline. Although we estimated the free [Ca^{2+}] in the layer whose dimensions extend horizontally 400 nm in both directions, the decline in concentration is over in less than 50 μs. This agrees well with a previous report showing that microdomains around channels triggering secretion dissipate in less than 100 μs [60]. In contrast a similarly rapid rise in the number of bound fixed buffers is followed by a slow decline. Furthermore, the number of bound fixed buffers continued to rise after the Ca^{2+} channel closed (Ca^{2+} entered only during first 50 μs), indicating that the binding of free Ca^{2+} to the unbound fixed buffers outweighs the unbinding of Ca^{2+} from the bound fixed buffers. This process was especially prominent in the vesicular presence especially with larger vesicles. A greater fraction of fixed buffers in the bound state increases Ca^{2+} unbinding and lowers the likelihood for Ca^{2+} binding to fixed buffers. Nevertheless binding of Ca^{2+} ions is much increased owing to the great rise in free [Ca^{2+}].

Increasing the affinity of fixed buffers tenfold had no discernible effect on the onset of Ca^{2+} binding to fixed buffers; the time course of the rise of the free [Ca^{2+}] and of the number of bound fixed buffers in the "first layer" remain similar irrespective of whether the forward rate was increased or the backward rate decreased (Fig. 6C). This is not surprising. The equilibration time of the fixed buffer is now relatively shorter than the diffusion time for Ca^{2+} across a region where most of the Ca^{2+} gradient occurs. A subsequent decline in the number of bound fixed buffers is however slower if the affinity is enhanced by lowering the backward rate. Any Ca^{2+} ion that becomes unbound is quickly captured by the available unbound buffers even at "control" forward rates, and increasing the rates does not alter the situation greatly. However, lowering the backward rates tenfold slows down Ca^{2+} unbinding proportionately and thus the offset time. All these differences become more pronounced if the affinity is reduced tenfold from the "control" level. The difference in the offset time becomes more pronounced, and if affinity is reduced by raising the backward rate the offset time of the occupancy of bound buffers approaches the offset time of free [Ca^{2+}]. Furthermore, in such a case the maximal occupancy of bound fixed buffers is much reduced.

Changes in the spatial distribution of bound fixed buffers near the plasma membrane and vesicular presence

Visual examination of the "snapshots" of bound fixed buffers in the first layer (Fig. 4B–D) shows that fixed buffers become quickly saturated close to the locus of Ca^{2+} entry. As Ca^{2+} continues to enter, saturation spreads laterally. The presence of vesicles clearly enhances the lateral spread of fixed buffer saturation. We quantified these changes in the lateral spread of saturated fixed buffers during and following brief pulses of Ca^{2+} flux in the presence and absence of vesicles. Saturation at any

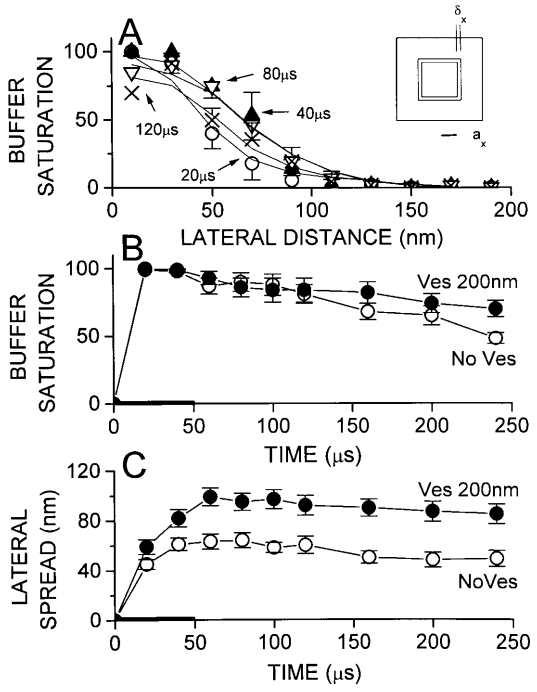

Fig. 7A–C Vesicular presence markedly alters the spatial profiles of bound fixed buffers near the plasma membrane. **A** Saturation of fixed buffers near plasma membrane at different times (as indicated) from the start of Ca^{2+} entry. The curves are best-fitted sigmoidal curves (no vesicle present). *Abscissa* – lateral distance from the locus of Ca^{2+} entry to the middle of the segment ($a_x+\delta_x/2$) where the saturation of fixed buffers was estimated (see the *inset*). **B** Time dependence of the maximal saturation (calculated as the asymptotic value of the fitted sigmoidal curves at zero distance), in the absence and presence of diffusion barrier (200×200 nm and positioned 15 nm from the plasma membrane). **C** Time course of the lateral spread of bound fixed buffers (estimated from the fitted sigmoidal curves as the distance between the locus of Ca^{2+} entry and the locus at which buffer saturation falls to 50% of its value at "zero distance")

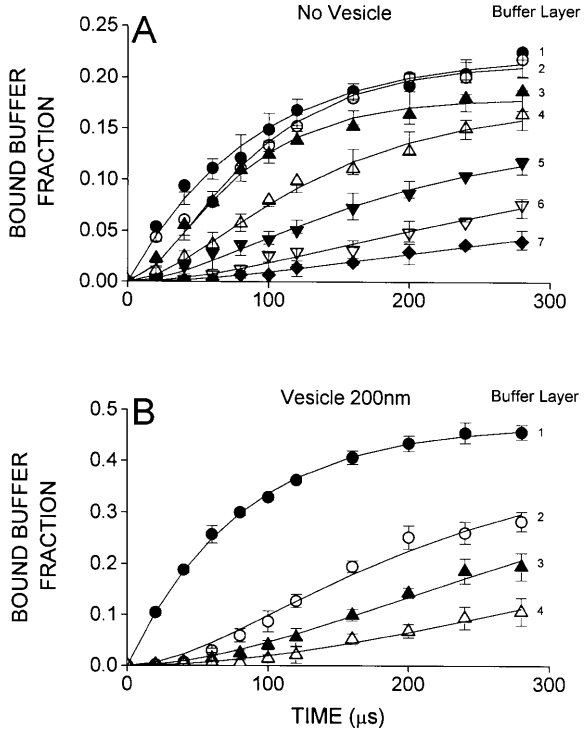

Fig. 8A, B The presence of vesicles profoundly alters the time course and the extent of Ca^{2+} binding to the bound fixed buffers near and far from the plasma membrane. Two cases are shown, no vesicle (**A**), and a vesicle (represented as a 200×200 nm flat diffusion barrier) positioned 15 nm above the plasma membrane (**B**). The layers of fixed buffers, each 16.7 nm thick, are enumerated progressively as the distance from the plasma membrane increases (*1* – closest; *12* – furthest). The best-fitted curves are a single exponential (defined by the equation $y=a\cdot[1-\exp(-t/\tau)]$, where a is the steady-state value of the number of bound fixed buffers and τ the time constant; first layer) or squared exponentials {defined by the equation $y=a\cdot[1-\exp(-t/\tau)]^2$, all other layers}

distance is calculated as the mean percentage of all bound fixed buffers in a rectangle (see inset of Fig. 7A), and the distance is calculated as $a_x+\delta_x/2$ where δ_x is the "collision length" of a single buffer molecule (16.7 nm at the buffer concentration of 367 μM). Evaluating the level of saturation in such a rectangle is preferred to evaluating it in an annulus, since the buffer molecules are arranged in a rectangular manner (see Simulation methods). The curves are best fitting sigmoids (calculated using the least-square methods). Figure 7B gives time course of maximal or "zero distance" saturation. The maximal saturation reaches the peak value very rapidly and decays, although slowly, following the cessation of Ca^{2+} entry. The decay is further prolonged in the presence of vesicles. In contrast the "lateral spread" (defined as the distance over which the buffer saturation decreases from its maximal value at the "zero distance" to 50% of the corresponding maximal value; Fig. 7C) continued to increase briefly following the cessation of Ca^{2+} entry and decreased but only slowly afterwards. The lateral spread is considerably greater in the presence of vesicles (its decay is however only marginally slower).

In-depth spread of binding to fixed buffers: effect of vesicular presence

The vesicular presence also profoundly changes the indepth spread of Ca^{2+} binding to the fixed buffers. Figure 8 gives the time course of the change in the total number (out of maximal 576) of bound fixed buffers in the layers above the plasma membrane (all individual layers are 16.7 nm thick, i.e., 12 layers span the whole simulation space). As expected, fixed buffers become first bound in the layers close to the plasma membrane. Vesicular presence however alters this binding process markedly. (A – no vesicle; B – vesicle; 200×200 nm flat infinitely thin diffusion barrier positioned 15 nm above the plasma membrane). Figure 9A gives the relationship between the number of bound fixed buffers and the vertical distance from the plasma membrane (evaluated 200 μs from the opening of the Ca^{2+} channel and the start of simulation; note the difference in the scales for the ordinate), and Fig. 9B gives the relationship between the time needed to reach the steady-state and the distance from the locus of Ca^{2+} entry. As expected: (1) fewer

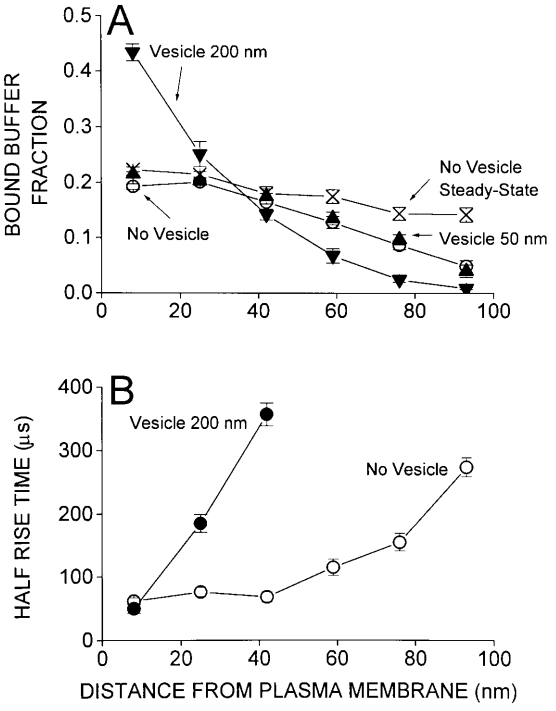

Fig. 9 **A** The in-depth spread of bound fixed buffers evaluated 200 μs from the start of simulation is markedly altered by the vesicular presence both near the plasma membrane and at greater depths. *Abscissa* – distance of individual fixed buffer layers (taken as the distance between the midpoint for each layer and the plasma membrane). *Ordinate* – number of bound fixed buffers in individual layers (maximal number is 576). The steady-state estimates of the bound buffers (*No vesicle*) are also shown (*crosses*). **B** The time needed for fixed buffers to become bound increases greatly as the in-depth distance increases. It is further prolonged by the vesicular presence (except for the "first layer" near the plasma membrane). Ca^{2+} flux was 5 ions/μs (equivalent to 1.6 pA) throughout the simulation

fixed buffers are bound further from the plasma membrane, and (2) it takes longer for binding to occur. The presence of vesicles enhances both trends in a size-dependent manner.

Discussion

Vesicles as barriers to Ca^{2+} diffusion: implications for quantal analysis

The aim of the present analysis was to develop a model to evaluate the changes in free [Ca^{2+}] near the plasma membrane and the locus of Ca^{2+} entry. Albeit a follow-up to several previous studies that evaluated Ca^{2+} dynamics near its locus of entry [13, 43, 56, 60, 76, 77], this study expands several important aspects of the problem. In our formulation the vesicles were an integral part of the simulations and the effect of their presence on [Ca^{2+}] was examined. Both the vesicular size and their distance from the plasma membrane were varied. Moreover, the effect of changing the single-channel Ca^{2+} flux and the fixed buffer (its concentration, affinity and kinetics) on Ca^{2+} dynamics were also evaluated. Finally the spatio-temporal distribution of fixed buffers (free and bound) was assessed concomitantly.

The binding of Ca^{2+} to fixed buffers was studied for several reasons. During fast synaptic transmission Ca^{2+} diffuses over very short distances (a few tens of nm) from the loci of Ca^{2+} entry to the release sites and it has been suggested that en route the buffers (fixed or mobile) do not capture a high proportion of initial Ca^{2+} [17, 60, 63]. At least in some cases however, it is clear that the importance of buffers in capturing Ca^{2+} cannot be ignored [56, 58]. In addition, an assessment of the spatial profiles of the bound fixed buffers following a Ca^{2+} pulse can provide valuable information about how the subsequent Ca^{2+} pulses will reach the threshold levels needed to initiate secretion. We thus included buffers in our simulations, but focused our attention only on fixed buffers. To be effective in capturing Ca^{2+}, mobile buffers have to be very mobile and very concentrated. Their concentration, however, in many secretory cells appears to be low. In chromaffin cells, the fixed buffers clearly predominate [43]. More importantly, the mobility of endogenous mobile buffers is low in chromaffin cells [78], as well as in the calyx of Held [37]. In the simulations of Ca^{2+} dynamics in neuroendocrine cells [43] and in hair cells [56] the diffusion constant of the endogenous mobile buffer was assumed to be 15 and 20 μ^2/s respectively. Such diffusion constants are compatible with calbindin, a Ca^{2+}-binding protein in neurons that is believed to play a role in Ca^{2+} buffering [36, 55, 56]. On the time scale of our simulations, the mobile buffers can be considered as fixed. The complex effects of mobile buffers on Ca^{2+} dynamics [56] will be the topic of a separate study.

Distortions of Ca^{2+} dynamics due to the vesicular presence were examined over a wide range of vesicular diameters (25–400 nm) and vesicle-plasma membrane distances (15–45 nm). Though vesicular diameters within a single type of secretory cell are typically not very variable, they can be very different from one type of cell to another. In central or peripheral synapses vesicular diameters average approximately 40–50 nm [12, 38]. In catecholamine-containing cells they are considerably larger. In chromaffin cells the mean vesicular diameters have been estimated to be 174–380 nm, with a coefficient of variation ranging from 0.3 to 0.65 (adrenaline-secreting cells); the corresponding values for norepinephrine-secreting cells are 210–292 nm and 0.58–0.87 [19, 34]. Vesicle-plasma membrane distances are also variable, even when considering only those that appear to be "docked". The shortest separation can be as little as a few nanometers [65]. Note that the focus of this study is how the Ca^{2+} dynamics are altered by the presence of vesicles of variable size, and on the evaluation of how such a presence alters vesicular secretion. However, vesicles cannot be positioned just anywhere, but have to be close to the "release loci". Furthermore, after being pre-docked they have to be primed to be converted into fully docked vesicles. These will be additional factors contributing to secretion.

The model yields several important insights into how Ca^{2+} dynamics are altered by the presence of vesicles and how such distortions may alter the mechanism of vesicular secretion. When the vesicles are close to the plasma membrane, during secretion they act as important barriers for the diffusion of free Ca^{2+} and significantly alter its sub-membrane spatial profiles of free $[Ca^{2+}]$ if Ca^{2+} is raised rapidly (as occurs during evoked release when one or several channels open synchronously). Greater accumulations of free $[Ca^{2+}]$ near larger vesicles situated close to the plasma membrane would tend to increase their probability of release during evoked release. In contrast, if Ca^{2+} increases slowly, or if it reaches the high levels needed for triggering the secretion owing to the contributions from entry sites over a large area of plasma membrane, or due to stochastic free $[Ca^{2+}]$ fluctuations (as during spontaneous release), vesicles will act to a lesser extent as barriers to Ca^{2+} diffusion, and the probability of release should then be less dependent of vesicular size. Therefore, evoked quanta are generally expected to have a greater quantal size than the spontaneously released quanta. The difference between their quantal sizes are expected to be greater than the differences of free $[Ca^{2+}]$ may suggest if the relationship between Ca^{2+} concentration and release follows the power law ([5, 61]; but see [60]), and owing to the cubic relationship between the vesicle's diameter and its volume. Note however, that if secretion is induced by Ca^{2+} release from internal stores, small vesicles would be released preferentially. Because they are less efficient diffusion barriers, they are less likely to prevent Ca^{2+} from reaching the high levels at the secretion loci.

Note that the term quantal size refers to "presynaptic quantal size" [68]. The changes of the postsynaptic receptor density, their desensitization and saturation that occur at synapses and influence "postsynaptic quantal size" can be ignored. To simplify the analysis we assumed that the intravesicular transmitter concentration was independent of the vesicular size. It remains controversial whether the intravesicular concentration is constant for a given type of secretory cell, and if not if it depends on vesicular size. Tight regulation of the intravesicular concentration in neuroendocrine cells has been suggested [27], but this has been contested [3]. It has also been argued that the concentration depends on vesicle size [34].

To further advance our understanding of how changes of conditions of secretion lead to the preferential release of vesicles of different sizes, we explored how varying the vesicle-independent free $[Ca^{2+}]$, or the slope of the vesicular diameter versus free $[Ca^{2+}]$ relationship alters the frequency distributions of released vesicles. Our simulations showed that: (1) the $[Ca^{2+}]$ accumulates more under large than small vesicles with larger single-channel Ca^{2+} flux, with greater vesicle-plasma membrane separation, and with higher concentration of fixed buffers, and (2) the vesicle-size-independent increase in free $[Ca^{2+}]$ rises with larger single-channel Ca^{2+} flux, but diminishes in the presence of buffers. We also varied the standard deviation/mean (CV) of the diameters of available vesicles, and assumed that the relationship between $[Ca^{2+}]$ and release probability was either sigmoidal or linear. Though the generality of conclusions based on such spatially restricted Ca^{2+} entry very near the locus triggering secretion is limited, they provide some insight into the extent of preferential release of different-sized vesicles.

Not unexpectedly the mean values and CVs of volumes of released and available vesicles became similar with a rise in vesicle-size-independent free $[Ca^{2+}]$, but similar changes were also observed with a greater dependence of free $[Ca^{2+}]$ on vesicular size. This may appear surprising, but a greater dependence of free $[Ca^{2+}]$ on vesicular size leads to higher levels of $[Ca^{2+}]$, and higher probability of release with a reduced dependence on free $[Ca^{2+}]$. The mean values of volumes of released vesicles were, as a rule, greater than those of available vesicles, whilst their variability was lower – a consequence of a clear though changing preference for the release of large vesicles. Because released and available vesicles differed more when the diameters of available vesicles had a higher CV, a similar change of Ca^{2+} dynamics results in larger changes of quantal size in neuroendocrine cells than in synapses. The extent of change of both means and CVs of volumes of released vesicles was strongly influenced by the probability of release versus free $[Ca^{2+}]$ relationship, but even for a linear relationship [60] the changes of means and CVs, though less pronounced, were evident.

Changes in Ca^{2+} dynamics due to vesicular presence and the preferential release of newly formed transmitter

The greater accumulation of free $[Ca^{2+}]$ expected for larger vesicles during evoked but not spontaneous quantal release will lead to the quantal sizes of these two types of release being different. It also creates a functional pool of vesicles that are "preferentially released" during evoked but not spontaneous release. A well established body of experimental evidence agrees well with these predictions. Biochemical studies have shown that newly formed transmitter is released preferentially in response to nerve stimulation or to increased extracellular $[K^+]$ in cat superior cervical ganglion [16], in Torpedo electric organ [23] and in guinea pig cerebral cortex [71]. In mammalian motor nerve terminals, the incorporation of newly formed false transmitter acetyl-monoethylcholine into vesicles also revealed large differences in the rate of incorporation [44]. The incorporation occurs much sooner for evoked release than for spontaneous release. If these differences in incorporation are entirely due to the distortion of Ca^{2+} dynamics by the vesicular presence it follows that: (1) even though in individual secretory cells the variability of vesicular diameters is not pronounced, it is still large enough to lead to a much higher probability of release of large vesicles, (2) as a consequence, small vesicles must wait a longer time

before their release, and (3) the quantal size of evoked release will be greater than the quantal size of spontaneous release.

The preferential release of large vesicles (for evoked release) necessitates a revision of the traditional view of the origin of synaptic depression. It argues that the synaptic depression resulting from high-frequency stimulation may to a significant extent be due to a decrease in the quantal size of evoked release, not paralleled by a comparable decrease in the quantal size of spontaneous release. Quantal size would decrease since the release of large vesicles will not be followed by the replenishment of similarly large vesicles, but by vesicles of average size. Some studies suggest indirectly that such a mechanism may be important at the Mauthner fiber-giant fiber synapse [39] and at the frog neuromuscular synapse [30, 31].

Vesicular presence and the spatial distribution of bound fixed buffers

It has long been known that the presence of fixed buffers can slow Ca^{2+} diffusion greatly [40, 66]. Furthermore, fixed buffers spatially restrict the rise in $[Ca^{2+}]$ to the areas close to their entry near the plasma membrane [51]. Thus bound fixed buffers can be considered as indicators of the history of Ca^{2+} diffusion and thus as "memory elements" [51, 77]. As this study shows, the presence of vesicles near plasma membrane markedly changes the spatial profiles of bound fixed buffers, largely restricting them to the region near the plasma membrane. The vesicular effect on the bound buffers (as for free $[Ca^{2+}]$) is greater the larger the vesicles and the closer their position to the membrane. Such changes in the spatial profiles of bound fixed buffers close to the secretion loci will affect the free $[Ca^{2+}]$ increase induced by subsequent Ca^{2+} entry and may also be an important factor in regulating use-dependent changes in quantal release, such as facilitation. Since fewer Ca^{2+} ions will be "wasted" on binding to the buffers, free $[Ca^{2+}]$ will rise to higher levels and will have a greater chance of reaching the threshold levels needed to initiate release. Considering that the bound fixed buffers can reach saturation levels and that the total concentration of fixed buffers is in hundreds of micromoles, the resulting difference in the free $[Ca^{2+}]$ in the critical areas close to the secretion loci can be very important. Since the bound fixed buffers will be more restricted to the areas near the plasma membrane the larger the vesicular size, this will contribute to make the release of large vesicles even more preferential.

These simulations assume that Ca^{2+} buffering is spatially uniform, but the regional differences in Ca^{2+} buffering may be important. These may be caused by spatial differences in the Ca^{2+} buffer concentrations, by differences in their kinetics and/or affinity or alternatively by the presence of fixed negative charges on the plasma membrane [1]. Tillotson and Gorman [70] have shown that regional differences in Ca^{2+} buffering exist and that buffering is strongest near the membrane.

In conclusion, when positioned for secretion, vesicles can be important barriers to $[Ca^{2+}]$ diffusion. As a consequence the changes of $[Ca^{2+}]$ dynamics determine not only the probability of release but also mean values and the variability of the volume of released vesicles and of quantal size. The preferential release of large vesicles is more likely to occur during a synchronous than during an asynchronous opening of Ca^{2+} channels. The quantal size of evoked and spontaneous release are thus generally expected to be different. All changes will be especially pronounced in neuroendocrine cells and in other secretory cells with large vesicles.

Acknowledgements This work was supported by the grants from the Heart and Stroke Foundation of Canada and Canadian Institutes of Health Research to M.I.G. Dr. K. Krnjevic and Dr. M. Guevara read the manuscript and made valuable comments. We thank Mr. John Fracassi and Mr. Jarrod Jogie for their assistance in the development and debugging of the algorithm.

References

1. Allan D, Kallen K-J (1993) Transport of lipids to the plasma membrane in animal cells. Prog Lipid Res 32:195–219
2. Allbritton NL Meyer T, Stryer L (1992) Range of messenger action of calcium ion and inositol 1,4,5-trisphosphate. Science 258:1812–1815
3. Anderson BB, Zerby SE, Ewing AG (1999) Calculations of transmitter concentration in individual PC12 cell vesicles with electrochemical data and a distribution of vesicle size obtained by electron microscopy. J Neurosci Methods 88:163–170
4. Artalejo CR, Perlman RL, Fox AP (1992) ω-Conotoxin GVIA blocks a Ca^{2+} current in bovine chromaffin cells that is not of the "classic" N type. Neuron 8:85–95
5. Augustine GJ, Charlton MP, Smith SJ (1987) Calcium action in synaptic transmitter release. Annu Rev Neurosci 10: 633–693
6. Bartol TM Jr, Land BB, Salpeter EE, Salpeter MM (1991) Monte Carlo simulation of miniature endplate current generation in the vertebrate neuromuscular junction. Biophys J 59:1290–1307
7. Bekkers JM (1994) Quantal analysis of synaptic transmission in the central nervous system. Curr Opin Neurobiol 4:360–365
8. Bekkers JM, Clements JD (1999) Quantal amplitude and quantal variance of strontium-induced asynchronous EPSCs in rat dentate granule neurons. J Physiol (Lond) 516:227–248
9. Bekkers JM, Stevens CF (1995) Quantal analysis of EPSCs recorded from small numbers of synapses in hippocampal cultures. J Neurophysiol 73:1145–1156
10. Bossu JL, De Waard M, Feltz A (1991) Inactivation characteristics reveal two calcium currents in adult bovine chromaffin cells. J Physiol (Lond) 437:603–620
11. Bossu JL, De Waard M, Feltz A (1991) Two types of calcium channels are expressed in adult bovine chromaffin cells. J Physiol (Lond) 437:621–634
12. Ceccarelli B, Hurlbut WP (1980) Vesicle hypothesis of the release of quanta of acetyl-choline. Physiol Rev 60:396–441
13. Chad JE, Eckert R (1984) Calcium domains associated with individual channels can account for anomalous voltage relations of Ca-dependent responses. Biophys J 45:993–999
14. Cherki-Vakil R, Ginsburg S, Meiri H (1995) The difference in shape of spontaneous and uniquantal evoked synaptic potentials in frog muscle. J Physiol (Lond) 482:641–650
15. Church PJ, Stanley E (1996) Single L-type calcium channel conductance with physiological levels of calcium in chick ciliary ganglion neurons. J Physiol (Lond) 496:59–68

16. Collier B (1969) The preferential release of newly synthesized transmitter by a sympathetic ganglion. J Physiol (Lond) 205: 341–352
17. Connor JA, Nikolakopoulou G (1982) Calcium diffusion and buffering in nerve cytoplasm. Lect Math Life Sci 15:79–101
18. Cooper RL, Winslow JL, Govind CK, Atwood HL (1996) Synaptic structural complexity as a factor enhancing probability of calcium-mediated transmitter release. J Neurophysiol 75: 2451–2466
19. Coupland RE (1968) Determining sizes and distribution of sizes of spherical bodies such as chromaffin granules in tissue sections. Nature 217:384–388
20. del Castillo J, Katz B (1954) Quantal components of the endplate potential. J Physiol (Lond) 124:560–573
21. Dennis M, Miledi R (1971) Lack of correspondence between the amplitudes of spontaneous potentials and unit potentials evoked by nerve impulses at regenerating neuromuscular junctions. Nature 232:126–128
22. Dennis M, Miledi R (1974) Characteristics of transmitter release at regenerating frog neuromuscular junctions. J Physiol (Lond) 239:571–594
23. Dunant Y, Gautron J, Israel M, Lesbats B, Manaranche R (1972) Les compartiments d'acetylcholine de l'organe electrique de la Torpille et leurs modifications par la stimulation. J Neurochem 19:1987–2002
24. Edwards FA, Konnerth A, Sakmann B (1990) Quantal synaptic transmission in the central nervous system: a patch clamp study of IPSCs in rat hippocampal slices. J Physiol (Lond) 430:213–249
25. Fatt P, Katz B (1952) Spontaneous subthreshold activity at motor nerve endings. J Physiol (Lond) 117:109–128
26. Fenwick EM, Marty A, Neher E (1982) Sodium and calcium channels in bovine chromaffin cells. J Physiol (Lond) 331:599–635
27. Finnegan JM, Pihel K, Cahill PS, Huang L, Zerby SE, Ewing AG, Kennedy RT, Wightman RM (1996) Vesicular quantal size measured by amperometry at chromaffin, mast, pheochromocytoma, and pancreatic β-cells. J Neurochem 66:1914–1923
28. Friauf E (1993) Transient appearance of calbindin-D28k-positive neurons in the superior olivary complex of developing rats. J Comp Neurol 334:59–74
29. Gamble E, Koch C (1987) The dynamics of free calcium in dendritic spines in response to repetitive synaptic input. Science 236:1311–1315
30. Glavinovic MI (1987) Synaptic depression in frog neuromuscular junction. J Neurophysiol 58:230
31. Glavinović MI (1995) Decrease of quantal size and quantal content during tetanic stimulation detected by focal recording. Neuroscience 69:271–281
32. Glavinović MI, Rabie HR (1998) Monte Carlo simulation of spontaneous miniature excitatory postsynaptic currents in rat hippocampal synapse in the presence and in absence of desensitization. Pflügers Arch 435:193–202
33. Glavinović MI, Rabie HR (1999) Monte Carlo evaluation of quantal release and analysis. Soc Neurosci Abstr 25:474p
34. Glavinović MI, Vitale ML, Trifaro JM (1998) Comparison of vesicular volume and quantal size in bovine chromaffin cells. Neuroscience 85:957–968
35. Gold JI, Bear MF (1994) A model of dendritic spine Ca concentration exploring possible basis for a sliding synaptic modification threshold. Proc Natl Acad Sci USA 91:3941–3945
36. Heizmann CV, Braun K (1992) Changes in Ca-binding proteins in human neurodegenerative disorders. TINS 15:259–264
37. Helmchen F, Borst JGG, Sakmann B (1997) Calcium dynamics associated with a single action potential in a CNS presynaptic terminal. Biophys J 72:1458–1471
38. Heuser JE, Reese TS (1973) Evidence for recycling of synaptic vesicle membrane during transmitter release at the frog neuromuscular junction. J Cell Biol 57:315–344
39. Highstein SM, Bennett MVL (1975) Fatigue and recovery of transmission at the Mauthner fiber-giant fiber synapse of the hatchet fish. Brain Res 98:229–242
40. Hodgkin AL, Keynes RD (1957) Movements of labelled calcium in squid giant axons. J Physiol (Lond) 138:253–281
41. Jonas P, Major G, Sakmann B (1993). Quantal components of unitary EPSCs at the mossy fibre synapse on CA3 pyramidal cells of rat hippocampus. J Physiol (Lond) 472:615–663
42. Kasai H (1993) Cytosolic Ca^{2+} gradients, Ca^{2+} binding proteins and synaptic plasticity. Neurosci Res 16:1–7
43. Klingauf J, Neher E (1997) Modeling buffered Ca^{2+} diffusion near the membrane: implications for secretion in neuroendocrine cells. Biophys J 7:674–690
44. Large WA, Rang HP (1978) Factors affecting the rate of incorporation of a false transmitter into mammalian motor nerve terminals. J Physiol (Lond) 285:1–24
45. Larkman AU, Jack JJB, Stratford KJ (1997) Quantal analysis of excitatory synapses in rat hippocampal CA1 in vitro during low-frequency depression. J Physiol (Lond) 505:457–471
46. Liao D, Jones A, Malinow R (1992) Direct measurement of quantal changes underlying long-term potentiation in CA1 hippocampus. Neuron 9:1089–1097
47. Llinas R, Sugimori M, Silver RB (1992) Microdomains of high calcium concentration in a presynaptic terminal. Science 256:677–679
48. Lohman C, Friauf E (1996) Distribution of the calcium-binding proteins parvalbumin and calretinin in the auditory brainstem of adult and developing rats. J Comp Neurol 367:90–109
49. Naraghi M, Neher E (1997) Linearized buffered Ca^{2+} diffusion in microdomains and its implications for calculation of $[Ca^{2+}]$ at the mouth of a calcium channel. J Neurosci 17:6961–6973
50. Neher E, Augustine GJ (1992) Calcium gradients and buffers in bovine chromaffin cells. J Physiol (Lond) 450:273–301
51. Nowycky MC, Pinter MJ (1993) Time courses of calcium and calcium-bound buffers following calcium influx in a model cell. Biophys J 64:77–91
52. Parsons TD, Coorsen JR, Horstmann H, Almers W (1995) Docked granules, the excotytotic burst, and the need for ATP hydrolysis in endocrine cells. Neuron 15:1085–1096
53. Paulsen O, Heggelund P (1994) The quantal size at retinogeniculate synapses determined from spontaneous and evoked EPSCs in guinea-pig thalamic slices. J Physiol (Lond) 480:505–511
54. Paulsen O, Heggelund P (1996) Quantal properties of spontaneous EPSCs in neurones of the guinea-pig dorsal lateral geniculate nucleus. J Physiol (Lond) 496:759–772
55. Popov S, Poo MM (1992) Diffusional transport of macromolecules in developing nerve processes. J Neurosci 12:77–85
56. Roberts WM (1994) Localization of calcium channels by a mobile calcium buffer in frog saccular hair cells J Neurosci 10:3664–3684
57. Robinson RA, Stokes RH (1955) Electrolyte solutions. Butterworths, London
58. Sala F, Hernandez-Cruz A (1990) Calcium diffusion modeling in a spherical neuron. Relevance of buffering properties. Biophys J 57:313–324
59. Silver RA, Traynelis RF, Cull-Candy SG (1992) Rapid-time-course miniature and evoked excitatory currents at cerebellar synapses in situ. Nature 355:163–1666
60. Simon SM, Llinas RR (1985) Compartmentalization of the submembrane activity during calcium influx and its significance in transmitter release. Biophys J 48:485–498
61. Sinha SR, Wu LG, Saggau P (1997) Presynaptic calcium dynamics and transmitter release evoked by single action potentials at mammalian central synapses. Biophys J 72:637–651
62. Smith GD (1996) Analytical steady state solution to the rapid buffering approximation near an open Ca^{2+} channel. Biophys J 71:3064–3072
63. Smith SJ, Augustine GJ (1988) Calcium ions active zones and synaptic transmitter release. Trends Neurosci 11:458–464
64. Souček B (1971) Influence of the latency fluctuations and the quantal process of transmitter release on the end-plate potentials' amplitude distribution. Biophys J 11:127–139
65. Steyer JA, Horstmann H, Almers W (1997) Transport, docking and exocytosis of single granules in live chromaffin cells. Nature 388:474–478

66. Stockbridge N, Moore JW (1984) Dynamics of intracellular calcium and its possible relationship to phasic transmitter release at the frog neuromuscular junction. J Neurosci 4:803–811
67. Stuenkel EL (1994) Regulation of intracellular calcium and calcium buffering properties of rat isolated neurohypophysial nerve endings. J Physiol (Lond) 481:251–271
68. Sulzer D, Pothos EN (2000) Regulation of quantal size by presynaptic mechanisms. Rev Neurosci 11:159–212
69. Tank DW Regehr WG, Delaney KR (1995) A quantitative analysis of presynaptic calcium dynamics that contribute to short-term enhancement. J Neurosci 15:7940–7952
70. Tillotson DL, Gorman ALF (1983) Localization of neuronal Ca^{2+} buffering near plasma membrane studied with different divalent cations. Cell Mol Neurobiol 3:297–310
71. von Schwarzenfeld I (1979) Origin of transmitters released by electrical stimulation from a small metabolically active vesicular pool of cholinergic synapses in guinea-pig cerebral cortex. Neuroscience 4:447–493
72. Wahl LM, Pouzat C, Stratford KJ (1996) Monte Carlo simulation of fast excitatory synaptic transmission at a hippocampal synapse. J Neurophysiol 75:597–608
73. Wahl LM, Jack JJB, Larkman AU, Stratford KJ (1997) The effects of synaptic noise on measurements of evoked excitatory postsynaptic response amplitudes. Biophys J 73:205–219
74. Wall MJ, Usowizc MM (1998) Development of the quantal properties of evoked and spontaneous synaptic currents at a brain synapse. Nature Neurosci 1:675–682
75. Winslow JL, Duffy SN, Charlton MP (1994) Homosynaptic facilitation of transmitter release in crayfish is not affected by mobile calcium chelators: implications for residual ionized calcium hypothesis from electrophysiological and computational analyses. J Neurophysiol 72:1769–1793
76. Wu YY, Tucker T, Fettiplace R (1996) A theoretical study of calcium micro-domains in turtle hair cells. Biophys J 71: 2256–2275
77. Yamada WM, Zucker RS (1992) Time course of transmitter release calculated from simulations of a calcium diffusion model. Biophys J 61:671–683
78. Zhou Z, Neher E (1993) Mobile and immobile calcium buffers in bovine adrenal chromaffin cells. J Physiol (Lond) 469: 245–273